



**HAL**  
open science

# Mass budget partitioning during explosive eruptions: insights from the 2006 paroxysm of Tungurahua volcano, Ecuador

Julien Bernard, Julia Eychenne, Jean-Luc Le Pennec, Diego Narváez

## ► To cite this version:

Julien Bernard, Julia Eychenne, Jean-Luc Le Pennec, Diego Narváez. Mass budget partitioning during explosive eruptions: insights from the 2006 paroxysm of Tungurahua volcano, Ecuador. *Geochemistry, Geophysics, Geosystems*, 2016, 17 (8), pp.3224 - 3240. 10.1002/2016GC006431 . hal-01637038

**HAL Id: hal-01637038**

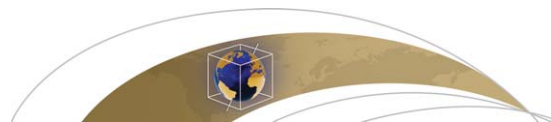
**<https://uca.hal.science/hal-01637038>**

Submitted on 20 Dec 2021

**HAL** is a multi-disciplinary open access archive for the deposit and dissemination of scientific research documents, whether they are published or not. The documents may come from teaching and research institutions in France or abroad, or from public or private research centers.

L'archive ouverte pluridisciplinaire **HAL**, est destinée au dépôt et à la diffusion de documents scientifiques de niveau recherche, publiés ou non, émanant des établissements d'enseignement et de recherche français ou étrangers, des laboratoires publics ou privés.

Copyright



## RESEARCH ARTICLE

10.1002/2016GC006431

## Mass budget partitioning during explosive eruptions: insights from the 2006 paroxysm of Tungurahua volcano, Ecuador

Julien Bernard<sup>1,2,3</sup>, Julia Eychenne<sup>1</sup>, Jean-Luc Le Pennec<sup>1,2,3</sup>, and Diego Narváez<sup>3</sup>

## Key Points:

- We determined the mass of all products (PDC, scoria fall, ballistics, lava) emplaced during the 2006 VEI3 eruption of Tungurahua (Ecuador)
- Most of the juvenile mass (44 wt. %) is for PDCs. Magma ascent, fragmentation and the crater area topography control the mass partitioning
- A literature review indicates that moderate andesitic eruptions produce more PDC in proportion than any other eruptions

## Correspondence to:

J. Bernard,  
j.bernard@opgc.univ-bpclermont.fr

## Citation:

Bernard, J., J. Eychenne, J.-L. Le Pennec, and D. Narváez Rivadeneira (2016), Mass budget partitioning during explosive eruptions: insights from the 2006 paroxysm of Tungurahua volcano, Ecuador, *Geochem. Geophys. Geosyst.*, 17, 3224–3240, doi:10.1002/2016GC006431.

Received 9 MAY 2016

Accepted 18 JUL 2016

Accepted article online 22 JUL 2016

Published online 11 AUG 2016

<sup>1</sup>Laboratoire Magmas et Volcans, Université Blaise Pascal - CNRS - IRD - OPGC, Campus Universitaire des Cézeaux, Aubière, France, <sup>2</sup>IRD, Alemania N32-188 y Guayanas, Aptdo 17-12-857, Quito, Ecuador, <sup>3</sup>Instituto Geofísico, Escuela Politécnica Nacional, Ladrón de Guevara E11-253, Aptdo. 2759, Quito, Ecuador

**Abstract** How and how much the mass of juvenile magma is split between vent-derived tephra, PDC deposits and lavas (i.e., mass partition) is related to eruption dynamics and style. Estimating such mass partitioning budgets may reveal important for hazard evaluation purposes. We calculated the volume of each product emplaced during the August 2006 paroxysmal eruption of Tungurahua volcano (Ecuador) and converted it into masses using high-resolution grain size, componentry and density data. This data set is one of the first complete descriptions of mass partitioning associated with a VEI 3 andesitic event. The scoria fall deposit, near-vent agglutinate and lava flow include 28, 16 and 12 wt. % of the erupted juvenile mass, respectively. Much (44 wt. %) of the juvenile material fed Pyroclastic Density Currents (i.e., dense flows, dilute surges and co-PDC plumes), highlighting that tephra fall deposits do not depict adequately the size and fragmentation processes of moderate PDC-forming event. The main parameters controlling the mass partitioning are the type of magmatic fragmentation, conditions of magma ascent, and crater area topography. Comparisons of our data set with other PDC-forming eruptions of different style and magma composition suggest that moderate andesitic eruptions are more prone to produce PDCs, in proportions, than any other eruption type. This finding may be explained by the relatively low magmatic fragmentation efficiency of moderate andesitic eruptions. These mass partitioning data reveal important trends that may be critical for hazard assessment, notably at frequently active andesitic edifices.

## 1. Introduction

Explosive volcanic events often lead to a variety of eruptive phenomena, including the effusion and extrusion of magma [e.g., *Watts et al.*, 2002; *Samaniego et al.*, 2011], as well as gravity- and buoyancy-controlled emplacement of fragmented material. Gravity-driven phenomena include ballistic ejections and generation of Pyroclastic Density Currents (PDCs), the latter encompassing *dense pyroclastic flows* (PFs) and *dilute pyroclastic surges* (PSs) [*Roche et al.*, 2013]. Convective and buoyancy-driven phenomena correspond to vent-derived and co-PDC (or coignimbrite) plumes, the latter referring to plumes that develop due to the rise of a hot mixture of particles and gas escaping from the body of PDCs [*Bonadonna et al.*, 2002; *Andrews and Manga*, 2012; *Engwell and Eychenne*, 2016]. Each of these phenomena represents specific hazards [e.g., *Branney and Kokelaar*, 2002; *Gurioli et al.*, 2005; *Horwell and Baxter*, 2006; *Guffanti et al.*, 2009; *Auker et al.*, 2013; *Jenkins et al.*, 2013; *Fitzgerald et al.*, 2014; *Kueppers et al.*, 2014], and generates deposits of contrasting geometry, texture and structure [e.g., *Walker*, 1971; *Pyle*, 1989; *Charbonnier and Gertisser*, 2011; *Gurioli et al.*, 2013]. Magma partitioning between different eruptive phenomena is controlled by the mechanisms of magma ascent and fragmentation processes in the conduit, as well as by ejection and transport dynamics of the erupted material. Deciphering the role of these processes in the eruption of the magma as effusive versus fragmented products, or as gravity- versus buoyancy-controlled phenomena, is critical to determine the likelihood of different eruptive scenarios [e.g., *Marzocchi et al.*, 2004]. High-resolution field data that document such partitioning are also essential to validate numerical and experimental models simulating the onset and behaviour of PDCs, such as the collapse of Plinian columns [*Neri et al.*, 2002; *Di Muro et al.*, 2004; *Carazzo et al.*, 2008] or the transfer of fragmented material and gas from PDCs to the atmosphere [*Andrews and Manga*, 2012; *Engwell and Eychenne*, 2016]. While these have long been recognized as critical issues in volcanology [*Rittmann*, 1962], studies that provide detailed eruptive partitioning data remain scarce; recent debates in the volcanology community, however, embolden efforts to suitably readdress this topic.

The size of volcanic eruptions is generally estimated using the volume or mass of material emitted (e.g., the volume-based *Volcanic Explosivity Index* (VEI) of *Newhall and Self* [1982] and the mass- and eruption-rate-based Magnitude and Intensity indexes of *Pyle* [2000]). Obtaining high-resolution volume estimates of eruptive products requires extensive and careful fieldwork, along with appropriate data processing. Various methods have been developed to determine volumes and masses of lava flows, PDC and tephra fall deposits [e.g., *Pyle*, 1989; *Fierstein and Nathenson*, 1992; *Wadge et al.*, 2006; *Charbonnier and Gertisser*, 2011; *Bonadonna and Costa*, 2012; *Eychenne et al.*, 2013]. Yet, volumes of eruptive products (classified as tephra and/or lava) have been quantified for less than 13% of eruptions listed in the Smithsonian database [*Siebert et al.*, 2011]. As a result, studies fully quantifying eruptive budgets are rare, and eruption sizes are commonly assessed solely using tephra fall deposits [*Siebert et al.*, 2011]. The bulk volume and mass of erupted products can differ appreciably from the magma production of an eruption, given that entrained nonjuvenile clasts, both accessory and accidental [*Cas and Wright*, 1987], may represent a significant proportion of pyroclastic deposits [*Bernard et al.*, 2014; *Brand et al.*, 2014].

The aim of this work is to investigate how the erupted material (juvenile or not) is partitioned between lava flows, ballistic, PDC and fallout deposits during a typical intermediate-size (VEI 3) andesitic eruption. The well-documented August 2006 eruption of Tungurahua volcano, Ecuador, offers a unique opportunity to estimate the volume and mass of a variety of eruptive products, and to assess partitioning metrics at an unprecedented level of resolution. The estimations obtained at Tungurahua are compared to published data for explosive events and for a wide range of magma compositions and eruption styles. We highlight the importance of PDC deposits in magmatic eruptive budgets, and provide recommendations to obtain improved magnitude-intensity estimates. Finally, the processes leading to the partitioning of the erupted magma into different explosive phenomena are discussed in terms of hazard assessment.

## 2. The 16 August 2006 Paroxysmal Eruption of Tungurahua

### 2.1. Eruptive Context and Phenomenology

The conical, 5023 m-high Tungurahua volcano, located 120 km south of Quito city in Ecuador (Figures 1a and 1b), started a new period of activity in 1999 after eight decades of dormancy, and remains active at the time of writing. From 1999 to early 2006, the activity alternated stages of quiescence with Strombolian to Vulcanian eruptive events. These events were characterized by the ejection of ballistic bombs and blocks, and hours- to weeks-long stages of ash fallout with local to regional impacts [*Arellano et al.*, 2008; *Le Pennec et al.*, 2012].

After 11 months of quiescence in 2005 and six subsequent months of intensifying eruptive activity in 2006, a notably stronger eruption took place on 14 July 2006 with emplacement of small-volume scoria flows and surges on the western flank of the edifice. The activity remained intense during the following weeks and culminated with a major andesitic Subplinian tephra fall- and scoria flow-forming event on 16 August 2006. This paroxysmal eruption was characterized by vigorous lava jetting and fountaining, the development of a 16–18 km-high above the vent eruption column [*Eychenne et al.*, 2012], and formation of numerous PDCs over 4 h [*Kelfoun et al.*, 2009; *Bernard et al.*, 2014]. A blocky lava flow descended the western flank as the explosive paroxysm waned [*Samaniego et al.*, 2011].

Combining seismic, acoustic and observational data, *Hall et al.* [2013] divided the August 2006 paroxysm into four phases. Phase I lasted about 12 h and consisted in low to moderate Strombolian activity (~0.5 km-high lava fountaining and ~1 km-high tephra columns). During the 3 h-long phase II, PDCs started to propagate down ravines on the western flank of the volcano, and the lava fountains' height reached 1.5 km. The paroxysmal phase III lasted 1 h, during which a sustained subvertical, vent-derived column developed, leading to substantial lapilli falls on the nearby communities and cities (e.g., Riobamba and Ambato) to the West. Elevated lava-fountaining activity continued and more PDCs were emplaced on the western, south-western and northwestern flanks of the volcano (Figure 1c). Phase IV corresponds to the extrusion of a lava flow pouring out the crater rim. The eruptive chronology is further detailed in *Arellano et al.* [2008], *Kelfoun et al.* [2009], *Fee et al.* [2010], *Steffke et al.* [2010], *Eychenne et al.* [2013], and *Hall et al.* [2013].

### 2.2. Eruptive Products

The poorly vesicular, andesitic lava flow field extends from the western crater rim down to ~2700 m a.s.l., a distance of ~3000 m (Figures 1c and 2a). Between elevations of ~3500 and ~2700 m a.s.l., the lava flow is channelled in separate gullies (Figure 2a).

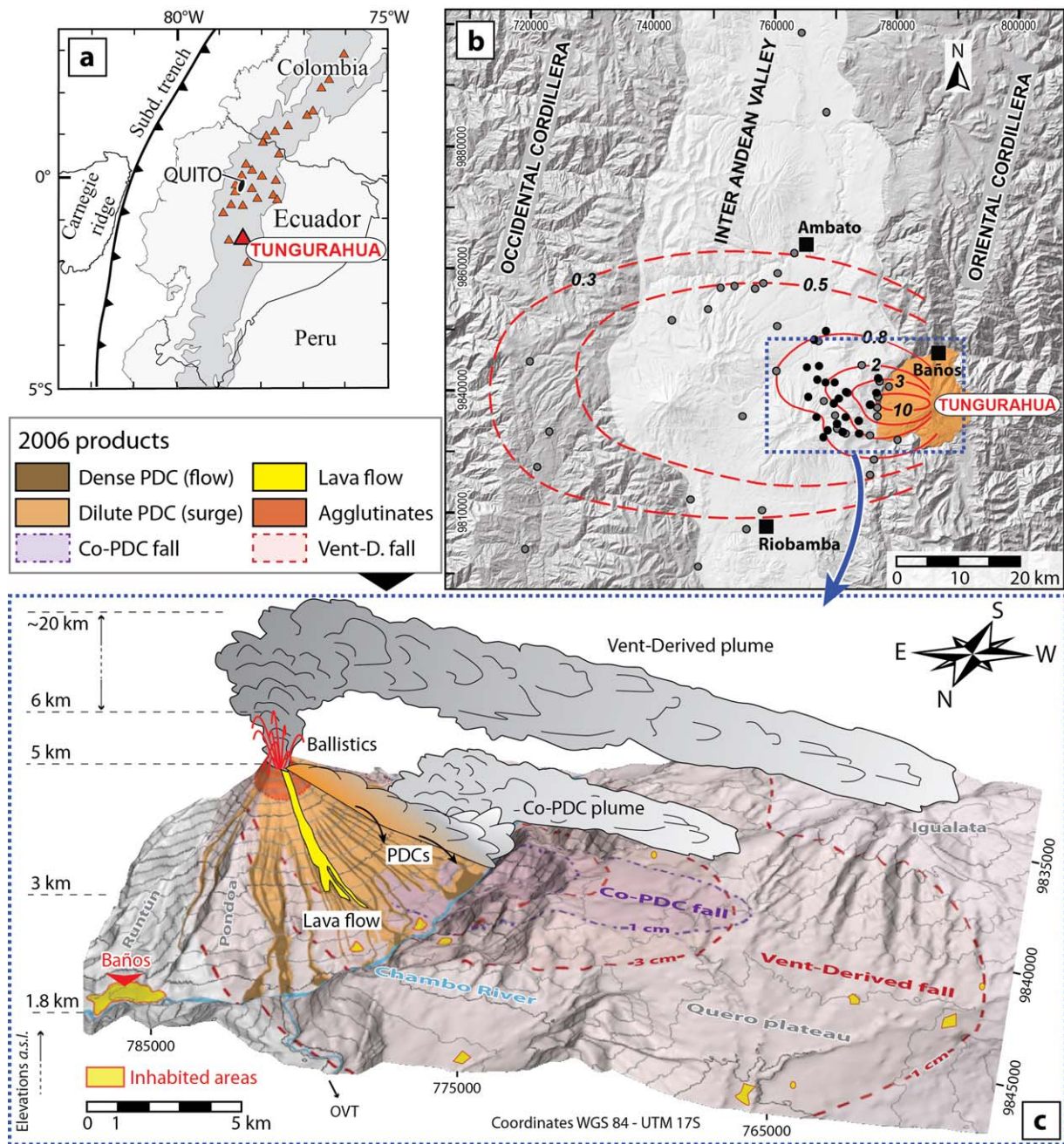


**Figure 1.** (a) General location map of Tungurahua volcano in Ecuador. The Andean topography above ~2000 m a.s.l. is shown in gray. Triangles represent volcanoes active during the past 10,000 years. (b) Close-up on the Tungurahua area displaying the edifice (in orange) and the isopachs (in centimetres) of the fallout deposit from the August 2006 eruption (from Eychenne *et al.* [2012]). The gray and black dots represent locations where the thickness and mass per unit area were determined, respectively. (c) Digital Elevation Model of the volcano (viewed from the North) representing the spatial distribution of the different product types emitted during the August 2006 eruption. PDC (Pyroclastic Density Current) encompasses both dense (pyroclastic flows, PF) and dilute (pyroclastic surges, PS) products. OVT indicates the location of the “Observatorio Vulcanológico del Tungurahua, Instituto Geofísico-Escuela Politécnica Nacional.”

Ballistic material (agglutinate, bombs and blocks) accumulated around the crater during the lava fountaining events and was visible on thermal images captured on 17 August by the Tungurahua Volcano Observatory (OVT) [e.g., Kelfoun *et al.*, 2009]. A significant fraction of the ballistic material was preserved at the end of the eruption as a red-tinted agglutinate on the inaccessible upper cone. Ground-based binoculars observations, and the interpretation of the thermal images, indicate that the agglutinate was restricted to elevations above ~4200 m a.s.l. (Figure 2a).

The PDCs were emplaced mainly on the western flank of the volcano (Figure 2a). The PF deposits were valley-confined in the ravine drainage network, and fan-shaped terraces at ravine openings (damming the

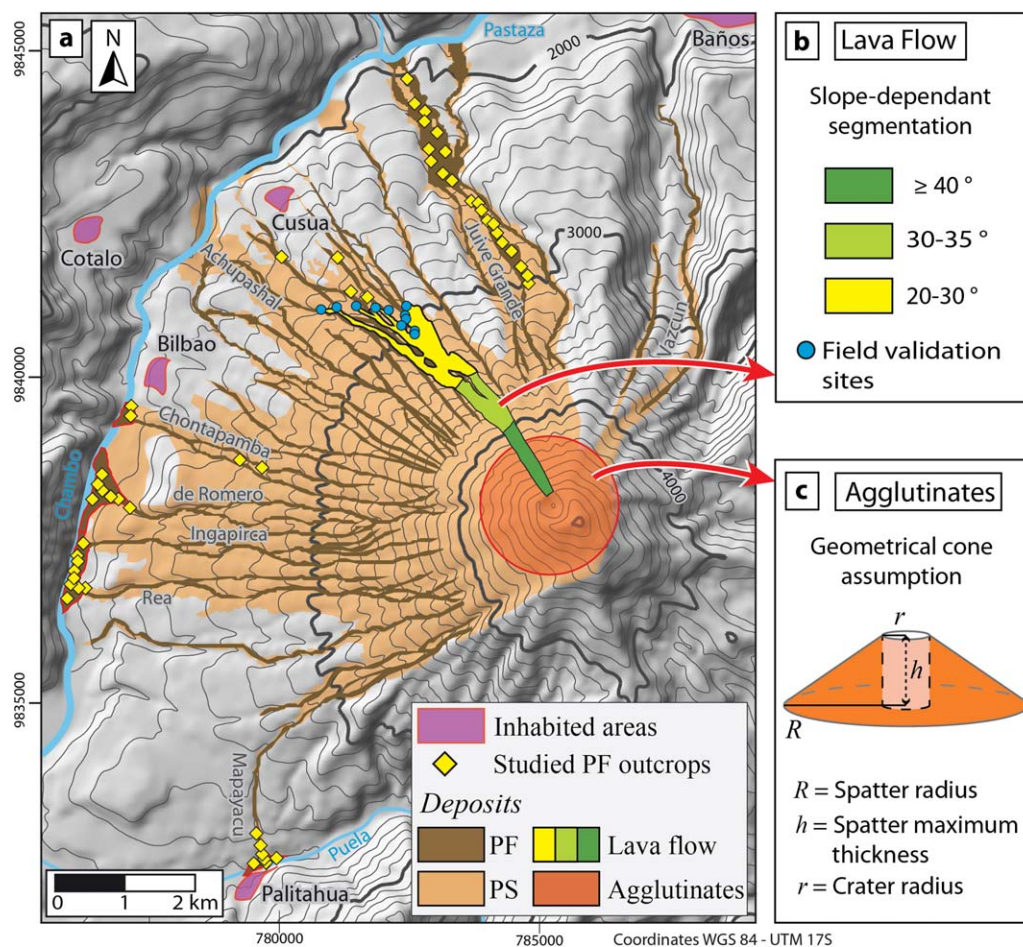


**Figure 2.** (a) Map of the August 2006 proximal eruption products (modified from Kelfoun *et al.* [2009] and Bernard *et al.* [2014]). Pyroclastic fans that formed in the Puela and Chambo rivers are outlined in red. Illustration of the volume calculation methods for (b) the lava flow and (c) the ballistic cone.

surrounding Chambo River (Figures 1c and 2a) [Hall *et al.*, 2013]. The valley-confined PF deposits are 2 to 7 m-thick on  $\sim 25^\circ$  proximal steep slopes and  $\sim 10^\circ$  more gentle distal slopes, respectively, with levee-and-channel structures [Hall *et al.*, 2013; Douillet *et al.*, 2013; Bernard *et al.*, 2014]. Fan-shaped terraces are 20–25 m thick, 500–1000 m wide (Figures 1c and 2a), and associated with a break-in-slope at the base of the volcanic edifice. The sequence of PF deposits consists of stacked flow units of coarsely grained (median grain size  $\sim 4$  mm) and poorly sorted material, with 30 to 50 wt. % of incorporated nonjuvenile products [Hall *et al.*, 2013; Bernard *et al.*, 2014]. The unconfined PS deposits cover a wide area (about 35 km<sup>2</sup>) on the western flank of the volcano (Figures 1c and 2a) and have a maximum thickness of 0.5–2 m. They appear as widespread laminated planar to cross-bedded, fine-grained and fairly well sorted lapilli and ash layers [Douillet *et al.*, 2013]. These PS deposits occur on top of and/or interbedded between PF units, and they blanket the volcano's flank between the main gullies, showing a gradational transition from flow to over-bank surge facies [Kelfoun *et al.*, 2009; Douillet *et al.*, 2013]. On the west side of the edifice a relatively thin (a few millimeters to  $\sim 20$  cm thick) distinct co-PDC deposit occurs on top of the PF and PS deposits as a massive and well sorted layer of very fine-grained ash (median grain size  $M_d \sim 40 \mu\text{m}$  [Eychenne *et al.*, 2012]).

A tephra fallout deposit of lapilli and ash covered an area of more than 3000 km<sup>2</sup> across the Inter-Andean Valley (Figure 1b) [Eychenne *et al.*, 2012, 2013]. On the volcano's flanks the tephra layer locally appears on top of, and intercalated within the sequence of PDC deposits. Beyond the PDC depositional area, the fallout deposit is unstratified and shows no vertical grading, despite containing both tephra from the vent-derived plume and ash from co-PDC plumes [Eychenne *et al.*, 2012]. This twofold contribution was revealed by the bimodal grainsize distributions of the fallout deposit, characterized by a coarse grained subpopulation

(from the vent-derived plume), whose median grain size decreases with distance from vent, and a fine grained subpopulation (from the co-PDC plumes), whose median grain size remains between 63 and 30  $\mu\text{m}$  over the studied area [Eychenne *et al.*, 2012; Engwell and Eychenne, 2016]. The term *fallout deposit* will refer hereafter to the mixed deposit comprising both a contribution from *co-PDC* and *vent-derived plumes*.

### 3. Methods to Determine the Eruptive Budget

#### 3.1. Lava Flow Field

The lower extents of each single tongue of the lava flow field were mapped below 3200 m a.s.l. soon after the eruption using a handheld GPS. Thickness of the lava fronts was measured at 13 locations. Geometry of the flow field in the upper part of the cone was determined using thermal and satellite images. To account for slope-dependent flow thickness we divide the lava flow field into three areas, each being of roughly constant slopes (Figures 2a and 2b): (1) between 2700 and 3500 m a.s.l. on the volcano's flank, the slope is 20–30° and we set a flow thickness between 8 m (maximum thickness measured at the lava flow front) and 4 m, (2) between 3500 and 4000 m a.s.l. the slope increases from 30 to 35° and a flow thickness of 4 to 2 m is assigned, and 3) above 4000 m a.s.l. where the slope is  $\geq 40^\circ$ , the flow thickness is set to 2–1 m. The mapped (i.e., vertically projected) flow area is corrected for the slope angle to calculate the total volume of the lava field. The mass of lava is determined assuming a DRE (Dense Rock Equivalent) density of 2650  $\text{kg}/\text{m}^3$  (pore-free andesite with 58%  $\text{SiO}_2$  Samaniego *et al.* [2011]), a bulk porosity (i.e., internal vesicularity and granular porosity) of 30%, and a juvenile content of 98 wt. %. The uncertainties on volume and mass estimates are determined in this study as the minimum and maximum values obtained by setting reasonable ranges of variation to the input parameters. Variations of the thickness of the lava flow along each segment lead to an uncertainty of  $\sim 33\%$  on the volume estimate.

#### 3.2. Ballistics Deposit

Based on observations and thermal monitoring data from the OVT, and following the method of Le Pennec *et al.* [2012], we approximate the geometry of the deposit of agglutinated ballistics to that of a truncated low cone of radius  $R = 1000 \pm 100$  m and of maximum thickness  $h$  between 5 and 10 m (i.e.,  $h = 7.5 \pm 2.5$  m). This cone is centred on the conduit, represented as a cylinder with a radius  $r = 100 \pm 10$  m (Figure 2). The volume  $V_b$  of this virtual cone is given by the expression:

$$V_b = 1/3\pi h \times (r^2 + rR + R^2) - \pi r^2 h.$$

Given that the PDCs most likely originated from the gravitational collapse of the agglutinate [Kelfoun *et al.*, 2009], we assume that the ballistic products are lithologically similar to the scoriaceous bombs and dense juvenile blocks present downslope in the PF deposits [Bernard *et al.*, 2014]. We assign a mean clast-density of 2000  $\text{kg}/\text{m}^3$  (intermediate between densities of scoriaceous bombs and dense blocks, i.e.,  $\sim 1700$  and  $\sim 2700$   $\text{kg}/\text{m}^3$ , respectively [Eychenne and Le Pennec, 2012]) and an inter-granular porosity of 15% to convert the estimated volume to mass. We assume that the proportion of juvenile ballistic products in the agglutinate is similar to that in the fallout deposit, i.e., 98 wt. % of juvenile material [Eychenne *et al.*, 2013]. The uncertainties expressed above for each geometrical parameters  $R$ ,  $r$  and  $h$  lead to a total significant uncertainty of  $\sim 50\%$  on the ballistic volume determination.

#### 3.3. PDC (PF and PS) Deposits

The volumes of PF deposits are generally estimated by multiplying the area they cover by a mean thickness [Alvarado and Soto, 2002; Saucedo *et al.*, 2002; Charbonnier and Gertisser, 2008], or using a series of slope-dependent thickness values [Charbonnier and Gertisser, 2011; Solikhin *et al.*, 2015]. In the case of Tungurahua volcano, we determine the area overlaid by valley-confined PF deposits with georeferenced satellite images (from ASTER-TERRA), maps from the literature [Kelfoun *et al.*, 2009; Samaniego *et al.*, 2011; Hall *et al.*, 2013], and field observations made in 2012–2013. The thickness of the PF deposits was measured at 23 outcrops from the base to the top of the Juive Grande valley (located on the Northwest side of the volcano, see Figure 2a), and the results are averaged for volume calculation [Charbonnier and Gertisser, 2008]. The volume of the fan-shaped structure is determined using a field laser-telemetry method. Forty to sixty measurement stations were implanted on each fan, levelled using a laser rangefinder TRUPULSE 360 (accuracy of  $\pm 0.3$  m for horizontal distances,  $\pm 1^\circ$  for azimuths and  $\pm 0.25^\circ$  for tilt) and georeferenced (WGS84, UTM 17S) using a GPS-localized base station (Figure 3). The thickness of the structure was estimated at each station by

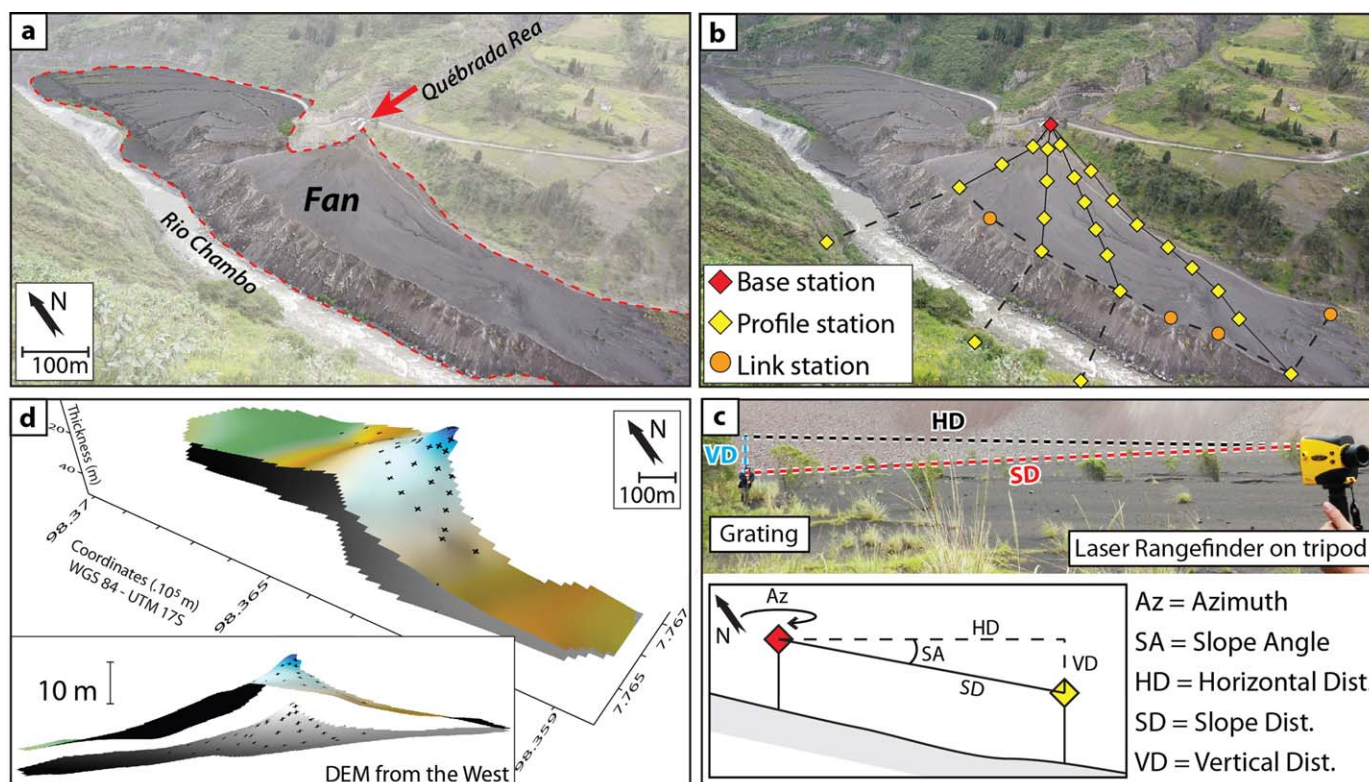


**Figure 3.** (a) Illustration of fan-like structure produced by the deposition of PF material in the Chambo river. (b) Example of distribution of the measurement stations along the southern part of the fan (the entire fan was covered). Projections across the river were used to reconstruct the distal portion of the fan that was eroded away by the Rio Chambo. The base station is georeferenced with a handheld GPS. (c) Illustration of data acquisition during the telemetric leveling. (d) DEM reconstruction of the base and the top of the fan structure for volume calculation (Surfer© software).

combining the apparent deposit thickness measured along recent, post-2006 ravines excavated down to the base of the fans, and pre-2006 georeferenced cartographic data. Digital Elevation Models (DEMs) of the top and basal surfaces of each fan are reconstructed (Surfer© software, kriging method) and used to determine the volume of each fan structure (Figure 3).

Grainsize and componentry distributions were determined for 26 samples collected in PF deposits from the western flank of the volcano (Figure 2a). The coarse fractions of the PF deposits (particles between 25.6 cm and 2 mm) were documented through the analyses of sets of high-resolution images taken orthogonally to each outcrop at different magnifications, whereas the fine fractions (particles between 16 mm and 63  $\mu\text{m}$ ) were determined through sample sieving and grain-counting methods [Bernard *et al.*, 2014]. 2-D clasts segmentation of numerical images according to textural criteria (shape, colour, aspect, etc.) allow the identification of 7 lithological families within the PF deposits (juvenile scoriaceous bombs, fragments and dense clasts; and nonjuvenile old lava, oxidized clasts, black scoriae and pumices, respectively; see Bernard *et al.* [2014]), and the determination of apparent 2-D grain size distributions. These 2-D data are converted into 3-D (volumes) using a stereological unfolded suite [Sahagian and Proussevitch, 1998; Shea *et al.*, 2010]. The grainsize and componentry mass distributions are then determined using proportions and densities of each componentry class identified in the deposits (see Bernard *et al.* [2014] for further detail on the method). This image- and sieve-based approach enables derivation of a single mass-based grainsize and componentry (between 25.6 cm and 63  $\mu\text{m}$ ). These high-resolution data, averaged over each studied gully, are used to (1) convert bulk volumes of deposits into masses, using a mean inter-granular porosity of  $13 \pm 6\%$  (inferred by measuring the compacted and noncompact volume of a known mass of each of the 26 PF samples), and (2) estimate the weight proportion of material recycled by the PFs during their emplacement (40 to 50 wt.% according to Bernard *et al.* [2014]), in order to assess the mass of the juvenile contribution in the deposits. The volume of the PS deposits is taken from Hall *et al.* [2013], and converted to mass assuming an intergranular porosity of 15% similar to the PF deposits, and a nonjuvenile material proportion of 15 wt. % [Douillet *et al.* 2013].

Considering an uncertainty of  $\pm 300$  m on the elevation of the site where PF sedimentation starts on the volcano's flank (i.e., mapping uncertainty) and an uncertainty of  $\pm 1$  m on the mean thickness, we obtain for PF valley-confined deposits a global volume uncertainty on the order of 29%. DEM-based fan volume calculations are mostly impacted by the accuracy of the rangefinder. By regularly returning to the reference station during measurement operations we determined a vertical and horizontal drift of about 1 and 14 m, respectively. This leads to an uncertainty of  $\sim 17\%$  on the global fan volume determination. Uncertainty related to the volume estimates of the PS deposits cannot be evaluated with data from *Hall et al.* [2013].

### 3.4. Fallout Deposit (Vent-Derived and Co-PDC Contributions)

The thickness and mass per unit area of the fallout deposit were measured at 59 (from  $\sim 7$  to 60 km from the vent) and 22 locations (from  $\sim 7$  to 20 km), respectively [*Eychenne et al.*, 2012, Figure 4], which allowed the reconstruction of the associated isopach [see *Eychenne et al.*, 2012] and isomass maps (Figure 4a). In order to document the thinning and mass decay rates of the deposit, individual isopach and isomass values are plotted against the square root of the area enclosed by the isolines (Figures 4c) [*Pyle*, 1989; *Fierstein and Nathenson*, 1992; *Bonadonna et al.*, 1998; *Bonadonna and Houghton*, 2005]. *Eychenne et al.* [2012] determined the volume of the fallout deposit by integrating the thinning rate fitted by an exponential law with two break-in-slope, as well as by a power law fit. From comparison of the results these authors concluded that the power law gives a reasonable minimum estimate of the deposit's volume when bounding the integration distally to 120 km [*Eychenne et al.*, 2012]. Here we use a power law to describe both the thinning and mass decay rates of the fallout deposit (see equations in Figure 4c), and calculate the total volume and mass of the deposit by integrating the functions between 1 km (maximum lateral extent of the agglutinate, see Figure 2a) and 120 km.

In order to separate the mass contributions of co-PDC ash and vent-derived tephra in the fallout deposit, we determine the mass per unit area of co-PDC ash in the proximal and medial area of the deposit (Figure 4b). Based on the detailed work presented in *Eychenne et al.* [2012], we consider that the fine subpopulation in the bulk grain size distributions of the fallout deposit samples corresponds to co-PDC ash, given that: (1) this fine subpopulation bear similar characteristics to the grain size of co-PDC products, and that (2) the fine ash enrichment trend within the fallout deposit occurs downwind of the main zone of PDC deposition on the western flank. Based on the weight proportion of the fine subpopulation determined by deconvolution [see *Eychenne et al.*, 2012, Figure 11] and details of the deconvolution method in the same paper), we assess the mass per unit area of the co-PDC contribution at 22 locations between  $\sim 7$  and 20 km from the vent. Isomass contours are drawn (Figure 4b), and their values are plotted against the square root of the isomass areas to describe the mass decay rate of the co-PDC contribution away from the vent (Figure 4c). The total mass of co-PDC ash in the fallout deposit is calculated by integrating the power law function fitting the co-PDC mass decay trend (Figure 4c) over an area: 1) starting at the first break-in-slope on the volcano's flank (slope decreasing to an angle of  $\sim 25^\circ$ ) where PF sedimentation began and likely triggered the formation of the main co-PDC plumes (i.e., between 2 and 3 km from the vent), and 2) extending to a distance similar to that selected for bounding the fallout deposit distally in the power law fit (i.e., 120 km from the vent). The mass of vent-derived tephra is inferred by subtracting the total mass of co-PDC ash to the total mass of the fallout deposit. Detailed componentry analyses performed in all the grain size fractions coarser than  $90 \mu\text{m}$  of the fallout samples showed that the deposit consisted of 98 wt. % of juvenile material [*Eychenne and Le Pennec*, 2012; *Eychenne et al.*, 2013]. This result is used here as a proxy to assess the juvenile contribution in the vent-derived fallout tephra. The mass of juvenile products in the co-PDC deposits is determined assuming that their componentry compares to that of the fine fraction ( $125$  to  $63 \mu\text{m}$ ) of the PDC materials.

The uncertainty related to the calculation of the tephra fallout volume is assessed using the Matlab package TError [*Bias et al.*, 2014], which allows the propagation of the uncertainty associated with thickness measurements, contouring isolines on a map, and using the power law integration method [*Bonadonna and Houghton*, 2005]. Based on Monte-Carlo simulations the code generates a distribution of volumes that accounts for the above uncertainties. The variability of the thickness data is determined as the standard deviation of 5 to 8 thickness measurements at a single location, and is between 17 and 2%. The uncertainty on isopach areas is determined following the results from *Klawonn et al.* [2014], as 30% for the two most distal isopach lines (displayed in Figure 1b), and 10% in the medial area of the deposit (7 to 20 km from vent). No proximal isopach lines were mapped due to the absence of thickness and mass per unit area measurements within 7 km from the vent. A fallout volume uncertainty of  $\sim 13\%$  is obtained considering

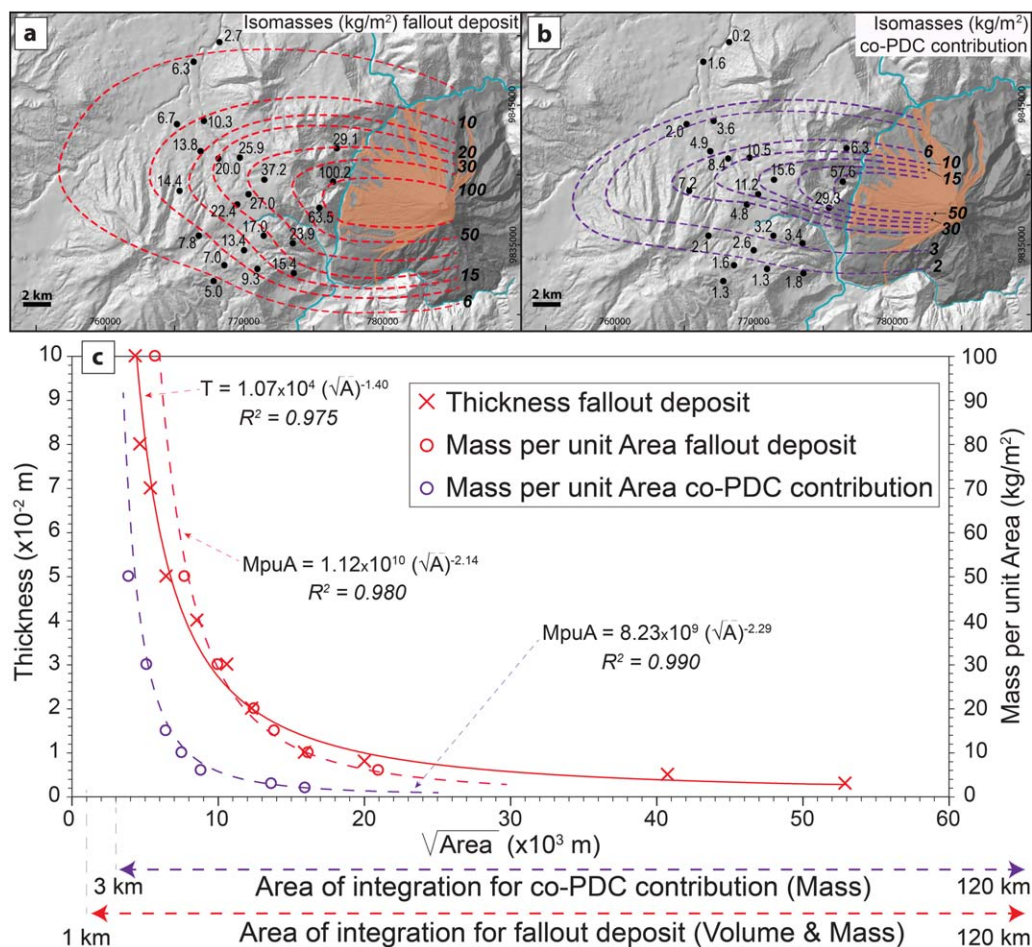


**Figure 4.** (a) Isomass map of the proximal area of the fallout deposit (including both the vent-derived tephra and co-PDC contribution) from the 16th of August 2006 Tungurahua eruption. (b) Isomass map of the contribution of co-PDC ash to the fallout deposit. The brown shaded area on the volcanic edifice represents the PDC deposits. (c) Plot of the thickness and mass per unit area versus square root of the isolines areas. The best power law fits through the different data points are represented, along with the area chosen for integrating the power law functions.

the 5<sup>th</sup> and 95<sup>th</sup> percentiles of the volume distribution. Because the mass estimates of the fallout deposit and the co-PDC contribution rely on the same field-based data and calculation methods, with their concomitant uncertainties, we assume that an uncertainty of 13% also applies to the mass results.

## 4. Eruptive Budget and Partitioning

### 4.1. Volume and Mass of the Eruptive Products

The *bulk* (i.e., including both juvenile and nonjuvenile material) volume and mass of the different product types of the August 2006 eruption are presented in Table 1. The bulk volume of all products is  $89.2 \pm 17.4 \times 10^6 \text{ m}^3$ , including  $\sim 39\%$  PDC deposits ( $\sim 26\%$  PF and  $\sim 13\%$  PS),  $\sim 44\%$  fallout deposits,  $\sim 10\%$  ballistics and  $\sim 7\%$  lava flow (Table 1). The fragmented (i.e., pyroclastic *sensu stricto*) material corresponds to  $83.2 \pm 15.4 \times 10^6 \text{ m}^3$ . Only the bulk volume of the fallout deposit (vent-derived and co-PDC contributions; Table 1) is estimated because the co-PDC contribution can be identified using solely the mass-based grain size data. The lava flow volume determined in this study ( $6.0 \pm 2.0 \times 10^6 \text{ m}^3$ ) is consistent with a previous estimate of  $\sim 7 \times 10^6 \text{ m}^3$  from Hall *et al.* [2013]. The bulk cumulated mass of the different product types is  $111.9 \pm 24.8 \times 10^9 \text{ kg}$ , with  $100.8 \pm 21.1 \times 10^9 \text{ kg}$  fragmented material (Table 1). This bulk mass divides up as  $\sim 10 \text{ wt. \%}$  lava flow,  $\sim 13 \text{ wt. \%}$  ballistics,  $\sim 52 \text{ wt. \%}$  PDC deposits ( $\sim 37 \text{ wt. \%}$  PF and  $\sim 14 \text{ wt. \%}$  PS), and  $\sim 25 \text{ wt. \%}$  fallout deposits ( $\sim 22 \text{ wt. \%}$  vent-derived tephra and  $\sim 3 \text{ wt. \%}$  co-PDC ash; Table 1 and Figure 5).

**Table 1.** Bulk Volumes, Masses and Juvenile Fractions of the Deposits for all the Six Different Products Emitted During the August 2006 Eruption of Tungurahua Volcano

	Bulk Volumes			Bulk Masses			Juvenile Masses	
	$\times 10^6 \text{ m}^3$	$\pm$	Vol.%	$\times 10^9 \text{ kg}$	$\pm$	wt.%	$\times 10^9 \text{ kg}$	wt.%
Pyroclastic Flows (PF)	23.5	5.7	26.3	41.7	9.6	37.3	21.0 <sup>a</sup>	24.0
Pyroclastic Surges (PS)	11.9 <sup>b</sup>		13.4	16.2		14.4	13.8 <sup>a,c</sup>	15.8
Co-PDC fall				3.6	0.5	3.3	3.1	3.6
Vent-derived fall	39.3	5.1	44.1	24.9	3.3	22.2	24.4 <sup>d</sup>	28.0
Ballistics	8.5	4.6	9.5	14.4	7.7	12.9	14.1	16.1
Lava flow	6.0	2.0	6.7	11.1	3.7	9.9	10.9	12.5
<b>Total</b>	<b>89.2</b>	<b>17.4</b>	<b>100</b>	<b>111.9</b>	<b>24.8</b>	<b>100</b>	<b>87.3</b>	<b>100</b>

<sup>a</sup>Componentry data from Bernard et al. [2014].

<sup>b</sup>Volume from Hall et al. [2013].

<sup>c</sup>Componentry data from Hall et al. [2013].

<sup>d</sup>Componentry data from Eychenne and Le Pennec [2012]. The "Total wt. %" column is the mass proportion of juvenile material emplaced during the eruption, which represent the mass partitionning.

### 4.2. Juvenile Material

The mass of juvenile products involved in the PDCs corresponds approximately to half of the mass of the PDC (PF and PS) deposits ( $34.8$  and  $57.9 \times 10^9 \text{ kg}$ , respectively), while the bulk masses of the fallout and ballistic deposits ( $28.5$  and  $14.4 \times 10^9 \text{ kg}$ , respectively) are close to those of their juvenile fractions ( $27.5$  and  $14.1 \times 10^9 \text{ kg}$ , respectively; Table 1 and Figure 5). The total mass of juvenile products emplaced during the eruption is about  $87.3 \times 10^9 \text{ kg}$ , 22% lower than the bulk mass of all product types (Table 1). Therefore, in terms of mass partitioning the juvenile fraction is shared as  $\sim 12 \text{ wt. \%}$  lava flow,  $\sim 16 \text{ wt. \%}$  ballistics,  $\sim 40 \text{ wt. \%}$  PDC deposits ( $\sim 24 \text{ wt. \%}$  PF and  $\sim 16 \text{ wt. \%}$  PS) and  $\sim 32 \text{ wt. \%}$  fallout deposits ( $\sim 28 \text{ wt. \%}$  vent-derived tephra and  $\sim 4 \text{ wt. \%}$  co-PDC ash; Table 1 and Figure 5).

### 4.3. Eruption Size

This updated and exhaustive eruptive budget is used here to reassess the size of the August 2006 Tungurahua eruption. The Volcanic Explosivity Index (VEI) [Newhall and Self, 1982] is estimated using both the bulk volume of the fragmented material produced by an eruption (as a proxy for the magnitude) and the height of the main vent-derived plume (as a proxy for the intensity). For the August 2006 Tungurahua event we determine the VEI from the volume of (Table 2): (1) the fallout deposit only (bulk volume  $V_b = 0.04 \text{ km}^3$ ), (2) all the fragmented product types (i.e., excluding the lava flow;  $V_b = 0.09 \text{ km}^3$ ), and (3) solely the juvenile fraction of the fragmented products ( $V_b = 0.07 \text{ km}^3$ ). Combined with a plume height of 16–18 km above the vent [Steffke et al., 2010; Eychenne et al., 2012], the volumetric results lead all to a VEI of 3 (Table 2).

Mass-based eruption size parameters are estimated using the definitions of the Magnitude ( $M = \log(\text{erupted mass in kg}) - 7$ ) and the Intensity ( $I = \log(\text{mass discharge rate in kg/s}) + 3$ ) of Pyle [2000]. We calculated these two parameters for (Table 2): (1) the fallout deposit only, (2) all the fragmented product types (i.e., excluding the lava flow), and (3) solely the juvenile fraction of the fragmented products. The magnitude  $M$  varies between 3.5 and 4.0, and the average mass discharge rate lies between  $2.0$  and  $7.0 \times 10^6 \text{ kg.s}^{-1}$

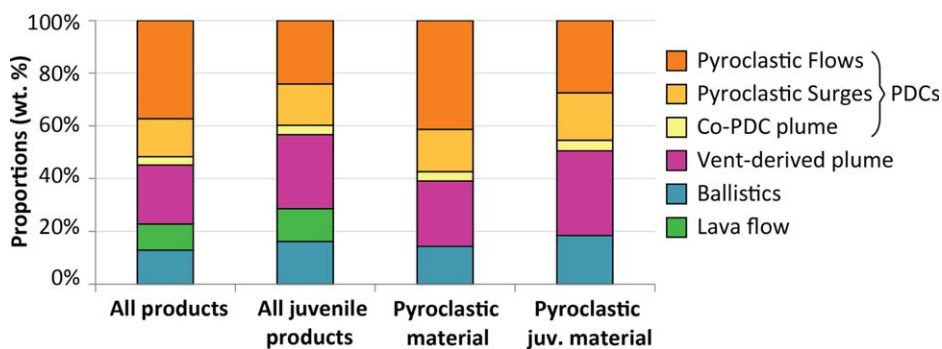


**Figure 5.** Histograms depicting the mass proportions (wt. %) of the eruptive products emplaced during the August 2006 eruption of Tungurahua (bulk, bulk juvenile, fragmented and juvenile fragmented material, respectively). PDC is for Pyroclastic Density Current (see text).

(considering a 4 h long paroxysm including Phase II and III, see section 2.1), yielding an intensity  $I$  between 9.3 and 9.8 (Table 2). The mass discharge rates estimated for all the fragmented products and separately for the juvenile material only are significantly higher than those obtained when using solely the mass of fallout deposit, leading to a  $>0.4$  increase of both  $M$  and  $I$  values (Table 2).

## 5. Discussion

### 5.1. Control of the Conditions of Magma Ascent and Fragmentation on Mass Partitioning

Considering that the PDCs were produced by gravitational collapse of the ballistic material accumulated as agglutinates upon the upper cone [Kelfoun *et al.*, 2009; Douillet *et al.*, 2013; Hall *et al.*, 2013; Bernard *et al.*, 2014], our budget results indicate that the August 2006 eruption of Tungurahua generated  $\sim 28$  wt. % efficiently fragmented juvenile material (vent-derived fallout with highly vesicular clasts in the sense of Houghton and Wilson [1989], i.e., 60–80% of vesicularity),  $\sim 60$  wt. % poorly fragmented magma (deposits of PDCs, co-PDCs and agglutinates), and  $\sim 12$  wt. % nonfragmented magma (lava flow; Figure 5 and Table 1). Most of the juvenile fragmented material ( $\sim 68$  wt. %, Figure 5) was erupted as ballistic products (scoriaeous bombs, dense juvenile blocks and coarse lapilli). A significant proportion of the juvenile ash produced by the eruption derived from co-PDC activity (i.e., 12 wt. % of the total mass of the tephra fall deposit and 4 wt. % of the mass of fragmented magma, Figure 5), and thus from secondary processes of fragmentation [Eycheenne *et al.*, 2013; Engwell and Eycheenne, 2016].

The poorly fragmented ballistic material should have been generated by the lava-fountaining activity, which lasted for the first three eruptive phases (representing 16 h of activity, see section 2.1). The more efficiently fragmented material is likely to have been produced during the 1 h-long paroxysmal phase III, while the sustained Subplinian column formed above the vent. These inferences raise fundamental questions about the conditions of magma ascent and fragmentation that controlled the contrasting eruptive styles during these different phases. The microlite content of the juvenile ash particles (supposedly produced during phase III and transported in the vent-derived column) showed variations from 4 to 67%, with an average value of 19%, suggesting a fast magma ascent rate of 13 m/s [Wright *et al.*, 2012]. Critically, the variability of the microlite content indicates a heterogeneity of the erupted magma batch. This may be related to relatively long-lasting timescales of magma intrusion (spanning throughout several days to a few weeks) within the shallow system prior to the 16 August eruption [Cashman, 1992], which implies variable durations of storage, and in turn to vertical variations of the microlite- and vesicle-content of the magma, as well as its permeability and density. Such a scenario concurs with the replenishment of Tungurahua's reservoir by a deep gas-rich magma batch, as inferred from analyses of mineral zoning and glass composition in juvenile products [Samaniego *et al.*, 2011]. The lava fountaining activity of phase I and II is consistent with the low energy bursting of a low viscosity, vesiculating magma batch ascending relatively slowly within the upper part of the conduit. Phase III in contrast, represents an acceleration of the eruption rate, and an increase of the fragmentation efficiency [Cashman and Scheu, 2015], which leads to the eruption of a microlite-poor and volatile-rich batch of magma. Yet, despite this increase in eruption intensity and the formation of the Subplinian column, the fragmentation remains heterogeneous during phase III, as suggested by the high

amount of ballistics associated with the lava fountaining activity, which fed the agglutinate deposit and led to an increased generation of PDCs. This heterogeneity of the fragmentation process can be related: (1) to a heterogeneity (both in terms of microlite and vesicle content) of the magma reaching shallow levels during phase III due, for example, to degassing of the magma along the conduit walls where permeability might be promoted [Jaupart and Allègre, 1991; Jaupart, 1998] rather than a simple vertically distributed heterogeneity [Burgisser *et al.*, 2010], or (2) to processes of ballistic

**Table 2.** Volume- (VEI) [Newhall and Self, 1982] and Mass-Based (Magnitude and Intensity) [Pyle, 2000] Size Estimation of the August 2006 Eruption of Tungurahua Volcano Using Different Types of Product<sup>a</sup>

	Fallout Deposit	All Fragmentation Products	Juvenile Fragmentation Products
Volume (km <sup>3</sup> )	0.04	0.09	0.07
Mass (10 <sup>9</sup> kg)	28.5	100.8	76.4
VEI	3	3	3
Discharge rate (10 <sup>6</sup> kg.s <sup>-1</sup> )	2.0	7.0	5.3
Magnitude	3.5	4.0	3.9
Intensity	9.3	9.8	9.7

<sup>a</sup>Only the fragmented products are considered for the determination of these parameters. Magnitude and Intensity are calculated considering an eruption duration of 4 h.

formation decoupled from the behaviour of the magmatic column (discussed in the next section). In both cases, the fragmentation level should have been relatively shallow during the different phases of the 2006 eruption. Seismic localization of the explosion sources during the recent activity of Tungurahua suggests that the fragmentation level is generally located 1 km below the crater [Battaglia *et al.*, 2015], which is consistent with the lack of metamorphic xenolith clasts in the 2006 products [Eychenne *et al.*, 2013]. The climactic phase ended with the effusion of the lava flow, indicating that the last batch of magma to be erupted was depleted in gas and had developed a high permeability in the upper conduit promoting gas escape [Le Pennec *et al.*, 2001; Rust and Cashman, 2011]. The lava represents a nonnegligible fraction of the emitted juvenile mass (14 wt. %), suggesting that the end of the explosive phase correlates with a decrease in gas content of the ascending magma rather than a strong reduction of the magma supply rate.

These interpretations, if correct, indicate that the eruption was overall dominated by sustained Strombolian activity (whereby relatively low viscosity magma bursts out), and that despite formation of highly vesicular scoriaceous bombs and lapilli clasts, the efficiency of the magmatic fragmentation was limited. Such an interpretation implies that the Total Grainsize Distribution of the fallout deposit alone [Bonadonna and Houghton, 2005] does not provide comprehensive information for the reconstruction of the fragmentation history of the eruption, limiting the extent to which the eruptive processes (magma ascent, explosivity, etc.) can be understood using only the fallout material [Kaminski and Jaupart, 1998; Rust and Cashman, 2011].

## 5.2. The Role of Topography on Mass Partitioning

According to our mass budget estimates, and assuming that gravitational destabilization of the agglutinate is the main process of PDC formation during this eruption [Kelfoun *et al.*, 2009; Hall *et al.*, 2013; Bernard *et al.*, 2014], about 73 wt. % of the ballistic material was remobilized to form PDCs (Table 1). Beyond the control of the processes of magma ascent and fragmentation, these results demonstrate that near-source topography can also play a significant role in the partitioning of eruptive products. Generation of PDCs by gravitational collapse of rapidly accumulated hot pyroclastic material at steep-sided andesitic stratovolcanoes has also been inferred from the 1975 Ngauruhoe eruption [Nairn and Self, 1978; Lube *et al.*, 2007], the 18 August and 16–17 September 1992 Crater Peak eruptions [Miller *et al.*, 1995], the 2013 Pavlof eruption [Waythomas *et al.*, 2014], as well as episodically at Arenal [Cole *et al.*, 2005] and Colima [“Soufrière-type” PFs of Saucedo *et al.* [2002]. In this context, the study of preserved agglutinate deposits generated by ballistic activity may bring valuable insights into the early generation mechanisms of PDCs, i.e., before syn-emplacement fragmentation and abrasion processes. In contrast, the accumulation of bombs and lapilli produced by ballistic activity leads to sheet-like deposits on flat to low-angle topographies (e.g., Stromboli, Italy, [Gurioli *et al.*, 2013]; 1992 eruptions of Crater Peak, Alaska, which accumulated dispersed blocks and bombs over a flat area around the vent [Miller *et al.* 1995]), or construct scoria cones (e.g., the 1943–1952 eruption of Parícutin, Mexico [Pioli *et al.*, 2008]; the 8.6 BP eruptions of La Vache et Lassolas, Chaîne des Puys [Jordan *et al.*, 2016]). Examples at Stromboli volcano (1930 paroxysm, and to a lesser extent during the 2003 and 2007 activity) also show that remobilization of large amounts of tephra accumulated on steep slopes may produce PDCs [Rosi *et al.*, 2006; Pistolesi *et al.*, 2011; Di Roberto *et al.* 2014], highlighting the important role of deposit thickness in ballistic- and slope-induced PDCs. Eruptions of similar magnitude and intensity thus appear to lead to different eruptive phenomena depending on vent morphology, crater configuration and edifice shape [Miller *et al.*, 1995]. This finding is of first importance for hazard assessment and risk mitigation purposes, especially in the case of steep-sided stratovolcanoes where moderate activity at the vent may translate into devastating PDC-forming events (e.g., 1968 eruption of Mayon, Philippines [Moore and Melson, 1969]; 1964 eruption of Gunung Agung, Indonesia [Self and Rampino, 2012]). Any change of near-vent topography should thus be closely monitored to anticipate the type of eruptive phenomena that may arise during background activity (e.g., flights above Tungurahua’s crater are repeatedly operated by the IG-EPN and partners in the context of routine surveillance duties; P. Ramon, com. Pers).

An alternative mechanism for the formation of PDCs could be related to the progressive filling of the crater by ballistic material accumulated during violent Strombolian episodes of lava fountaining prior to the paroxysm. Crater filling likely promotes overflowing of coarse material beyond the crater rim, thus leading to increased generation of PDCs. The time required to fill the crater should therefore relate to the intensity of PDC generation; such information may prove relevant for volcanic crises management purposes. The August 2006 paroxysm of Tungurahua was preceded by months of variably intense Strombolian to violent-Strombolian activity, which may have progressively filled the deep pre-August 2006 crater. The presence of

steep-sided crater walls during lower intensity lava fountaining events (e.g.,  $I = 6.5\text{--}7.0$  during the 2001 eruption of Tungurahua [Le Pennec *et al.*, 2012]), might have prevented the ejection of large amounts of ballistic material on the volcano slopes, thus modifying the mass partitioning of the eruptive products.

Erosion of the substrates on the volcano's flanks and incorporation of nonjuvenile material within the PDC during its emplacement may significantly change the final eruptive budget, particularly at Tungurahua where most of the mass was deposited by the PDCs. The erosive capacity of PDCs has been recognized at several volcanoes [e.g., Sparks *et al.*, 1997; Saucedo *et al.*, 2004; Lube *et al.*, 2007; Brand *et al.*, 2014], and a quantitative estimation shows that the amount of incorporated nonjuvenile material can represent up to 40–50 wt. % of the final deposits [Bernard *et al.*, 2014].

### 5.3. Implications for Size Assessment and Dynamics of the 2006 Tungurahua Eruption

The size of volcanic eruptions varies significantly from bulk volume- to mass-based estimates, and depending on which products are accounted for (Table 2). This is owed to the contrasting bulk density of PF deposits (typically between 1500 and 2000 kg.m<sup>3</sup> [e.g., Yamamoto *et al.*, 1993; Pyle, 2000]) and fallout deposits (typically between 700 and 1200 kg.m<sup>3</sup> [e.g., Sarna-Wojcicki *et al.*, 1981; Rose *et al.*, 2008; Eychenne *et al.*, 2013; Bernard, 2013]). Our high-resolution mass budget results demonstrate that the juvenile fraction in the fallout deposit represents only ~28 wt. % of the magmatic production of the August 2006 paroxysm of Tungurahua, suggesting that the fallout layer alone does not fully depict the size, dynamics, and fragmentation history of this explosive eruption (Figure 5). With ~44 wt. % the juvenile magma (including the ~4 wt. % co-PF deposits, Table 1, Figure 5) the PDC deposits may contribute significantly to the magmatic budget of that eruption, thus increasing the Magnitude and Intensity values (Table 2). This outcome highlights the potential importance of including PDC deposits in VEI determination, which is not always the case [Brown *et al.*, 2014], in order to faithfully describe the size of moderate eruptions, notably at andesitic stratovolcanoes. A recent work on ignimbrites reports mass partitioning ratios of 1:1:1 between PDCs, co-PDC and tephra fall deposits, thus emphasizing the crucial contribution of PDC deposits in mass budget of large-scale explosive eruptions too [Cook *et al.*, 2016].

### 5.4. Role of Magma Composition and Eruptive Style on Mass Partitioning

Published high resolution mass data of the different product types emplaced during eruptions are fairly rare. We compare here our results from the August 2006 eruption of Tungurahua with those obtained at other PDC-forming eruptions varying in style and magma composition. We carefully selected studies of recent well-preserved and well-documented explosive events presenting reliable PDC and tephra fall volumes, in order to assess meaningful ratios of PDC versus fallout volumes (hereafter referred as P/F ratios). Our compilation encompasses a selection of basaltic, andesitic and felsic eruptions, from violent Strombolian to Plinian, with VEI varying from 2 to 6 (Figure 6). Explosive basaltic eruptions rarely generate PDCs, as testified by their low mean P/F ratio of 0.06 (Figure 6). High P/F ratios are produced by andesitic eruptions, which tend to generate PDC deposits more voluminous than the tephra fall layers (mean ratio of 1.01, Figure 6). More felsic magmas are generally associated with large volumes of fallout and PDC deposits, but the PDC contribution is relatively minor with a mean ratio value of 0.29 (Figure 6). Most of the highest P/F ratios appear to be associated with small to moderate (VEI < 4) andesitic eruptions (mean ratio of 1.4, Figure 6). The notable 2010 Merapi exception suggests that large dome-forming eruptions may produce significant proportions of PDCs.

These contrasting ratio values can be explained by the highly efficient magmatic fragmentation of the large eruptions (both andesitic and felsic). The gas-particle mixtures produced during these events are generally more buoyant than moderate andesitic eruptions due to a higher gas content, a higher eruption rate, or the lower density of the clasts [Wilson and Walker, 1987; Jaupart and Allègre, 1991], thus favouring the partitioning of the erupted material toward plumes and tephra fall deposits. PDCs associated with felsic eruptions are commonly generated by the partial collapse of the eruptive column [Sparks and Wilson, 1976; Branney and Kokelaar, 2002; Carazzo *et al.*, 2015], whereas PDCs formed during moderate andesitic eruptions are associated with abundant ballistic projections, due to a lower efficiency of the magmatic fragmentation, as discussed above as well as reduced drag capacity of the jet related for example to lower ejection velocities. For past eruptions however, the volume of PDC deposits could be underestimated due to a poor preservation potential of the deposits. This may explain in some cases the low proportion of PDC deposits (e.g., pre-historical eruptions of Cotopaxi and Vesuvius volcanoes, see Figure 6), calls into question the robustness of

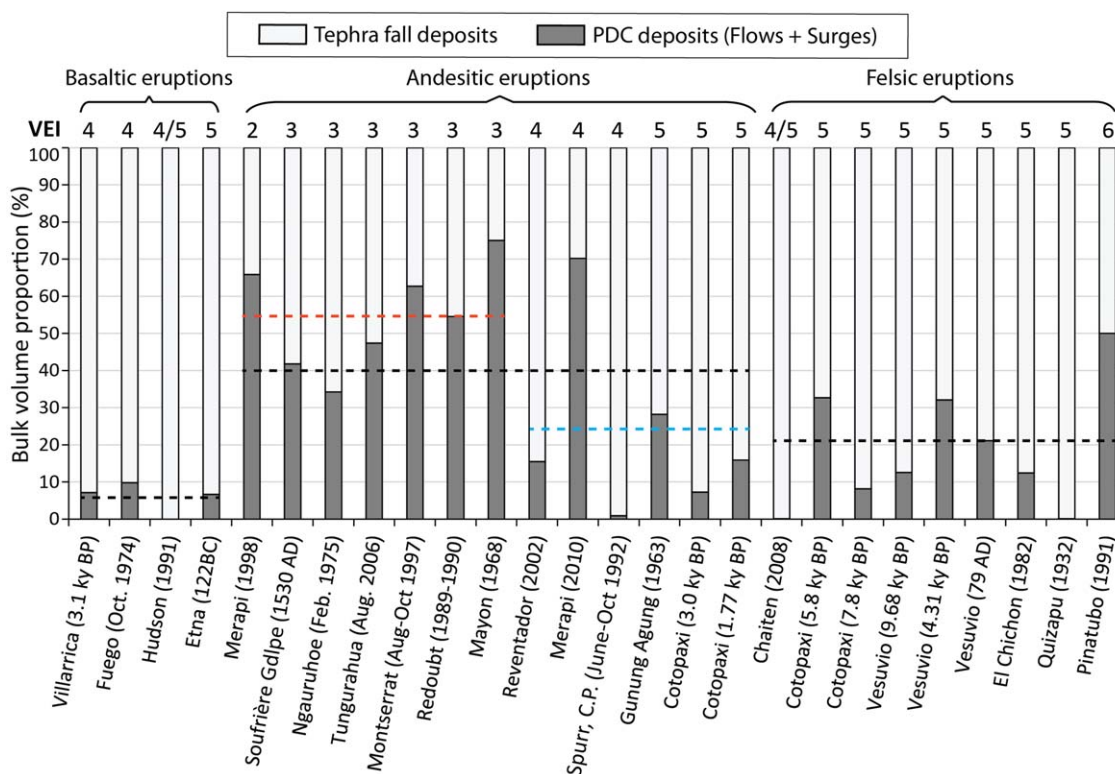


**Figure 6.** Bulk volumes of PDC versus tephra fall deposits for a variety of eruptions sorted by size (VEI). This compilation includes only reliable data available in the literature for basaltic, andesitic and felsic eruptions. The black dashed line represents the mean proportion (vol. %) of PDCs produced for each group of eruptions. The red and the blue dashed lines are the mean proportions (vol. %) of PDCs produced by moderate (VEI < 4) and large (VEI ≥ 4) andesitic eruptions, respectively. Data source: Villarrica [Costantini et al., 2011]; Fuego [Davies et al., 1978; Rose et al., 2008]; Hudson [Scasso et al., 1994]; Etna [Coltelli et al., 1998]; Merapi [Schwarzkopf et al., 2005]; La Soufrière de Guadeloupe [Komorowski et al., 2008]; Ngauruhoe [Nairn and Self, 1978]; Tungurahua, this study; Soufrière Hills Monserrat [Druitt et al., 2002; Bonadonna et al., 2002]; Redoubt [Scott and McGimsey, 1994; Gardner et al., 1994]; Mayon [Moore and Melson, 1969]; Reventador [Hall et al., 2004]; Merapi, 2010; [Charbonnier et al., 2013; Solikhin et al., 2015]; Mount Spurr - Crater Peak [Miller et al., 1995; McGimsey et al., 2001]; Gunung Agung [Self and Rampino, 2012]; Cotopaxi [Hall and Mothes, 2008]; Chaiten [Alfano et al., 2011; Major and Lara, 2013]; Vesuvio [Gurioli et al., 2010]; El Chichon [Sigurdsson et al., 1984; Carey and Sigurdsson, 1986; Sigurdsson et al., 1987]; Quizapu [Hildreth and Drake, 1992]; Pinatubo [Scott et al., 1996; Wiesner et al., 2004]. VEI from Siebert et al. [2011].

the volume estimation methods. Moreover, the emplacement of small-volume PDC deposits into preeruptive topographic depressions potentially results in their fast remobilization by lahars, introducing bias for volume determination [e.g., Cobeñas et al., 2014].

The trend of P/F ratio revealed by our compilation highlights that although Plinian events produce large volumes of products, moderate andesitic eruptions seemingly promote PDC formation, notably at steep-sided edifices. Since PDCs are the deadliest hazard of the last century [Tanguy et al., 1998; Auker et al., 2013], and because moderate andesitic eruptions are more frequent than large felsic events [Siebert et al., 2011], these findings have significant implications for hazard assessment and deserve further investigation.

### 6. Conclusion

We estimated the mass partitioning of all the different product types emplaced during the August 2006 paroxysm of Tungurahua volcano, Ecuador, using high-resolution volume determinations, volume-to-mass conversions and componentry corrections. The resulting data set is one of the first comprehensive, quantitative appraisals describing how the mass of volcanic products are distributed during a single violent-Strombolian to Subplinian VEI 3 event. From a methodological point of view, our work highlights the need to improve our ability to estimate PDC and ballistics volume and mass, and to reduce the associated uncertainties. The development of standardized methods similar to those recently developed to calculate the volume and mass of fallout deposits [e.g., Bonadonna and Costa, 2012; Eychenne et al., 2013] appears to be of primary importance.

Our partitioning results indicate that most of the juvenile erupted mass was emplaced as PDC products (~44 wt. % including deposits of dense PFs, dilute PSs and ash from co-PDC plumes). The tephra fall deposit

represents only ~28 wt. % of the juvenile magma (~32 wt. % including the co-PDC contribution), and alone depicts thus inadequately the whole dynamics and size of the studied event. Moreover, the ballistic material and lava flow each represent significant fractions of the juvenile magma (~16 and 12 wt. % of the total mass, respectively). These results stress the importance of considering all products for eruption size estimation (VEI, Magnitude and Intensity), and not only the tephra fall deposits. Our work can thus be used as a guideline for future studies, in particular for moderate PDC-forming eruptions.

Primary fragmentation and the conditions of magma ascent in the conduit (vesicularity, permeability, crystallinity) control the size and density of the clasts produced during the eruption and thus their partitioning toward the vent-derived plume (for relatively small clasts of low density) or the proximal ballistic-fed agglutinates (for larger and denser fragments), which have subsequently formed the PDCs. The near-vent topography may favour the production of PDCs by gravitational destabilization of hot syn-eruption agglutinates, particularly unstable on steep-sided proximal slopes. Finally, comparisons with other well-documented eruptions reveal that moderate andesitic eruptions have a higher P/F ratio than felsic and/or larger events. This finding is of first interest for hazard assessment, notably at frequently active steep-sided andesitic edifices where significant PDC production may occur during moderate volcanic eruptions.

### Acknowledgments

This work is part of JB PhD project, and has been completed in the context of a French-Ecuadorian cooperation program. We thank the Laboratoire Mixte International of IRD "Séismes et Volcans dans les Andes du Nord" for financial support. We warmly thank Josh Feinberg for editorial handling as well as Robert McGimsey and an anonymous referee for their constructive reviews, which greatly improved this paper. The authors also acknowledge Thierry Menand and Sébastien Leibrandt for their assistance during fieldwork in 2013. Data can be found within manuscript and references or from corresponding author upon request. This is Laboratory of Excellence ClerVolc contribution n°209.

### References

- Alfano, F., C. Bonadonna, A. C. Volentik, C. B. Connor, S. F. Watt, D. M. Pyle, and L. J. Connor (2011), Tephra stratigraphy and eruptive volume of the May, 2008, Chaitén eruption, Chile, *Bull. Volcanol.*, *73*, 613–630.
- Alvarado, G. E., and G. J. Soto (2002), Pyroclastic flow generated by crater-wall collapse and outpouring of the lava pool of Arenal Volcano, Costa Rica, *Bull. Volcanol.*, *63*, 557–568.
- Andrews, B. J., and M. Manga (2012), Experimental study of turbulence, sedimentation, and coignimbrite mass partitioning in dilute pyroclastic density currents, *J. Volcanol. Geotherm. Res.*, *225–226*, 30–44.
- Arellano, S. R., M. Hall, P. Samaniego, J. L. Le Pennec, A. Ruiz, I. Molina, and H. Yepes (2008), Degassing patterns of Tungurahua volcano (Ecuador) during the 1999–2006 eruptive period, inferred from remote spectroscopic measurements of SO<sub>2</sub> emissions, *J. Volcanol. Geotherm. Res.*, *176*, 151–162.
- Auker, M. R., R. S. J. Sparks, L. Siebert, H. S. Crossweller, and J. Ewert (2013), A statistical analysis of the global historical volcanic fatalities record, *J. Appl. Volcanol.*, *2*, 1–24.
- Battaglia, J., J. Hartmann, S. Hidalgo, J.-M. Douchain, J. Cordova, A. P. Alvarado, M. C. Ruiz, and R. Parra (2015), Location and Waveform Classification of Seismicity at Tungurahua Volcano (Ecuador) During the February and April 2014 Eruptive Phases, Abstract presented at 2015 Fall Meeting, AGU, San Francisco, Calif.
- Bernard, B. (2013), Homemade ashmeter: A low-cost, high-efficiency solution to improve tephra field-data collection for contemporary explosive eruptions, *J. Appl. Volcanol.*, *2*, 1–9.
- Bernard, J., K. Kelfoun, J.-L. Le Pennec, and S. V. Vargas (2014), Pyroclastic flow erosion and bulking processes: Comparing field-based vs. modeling results at Tungurahua volcano, Ecuador, *Bull. Volcanol.*, *76*, 1–16.
- Biass, S., G. Bagheri, W. Aeberhard, and C. Bonadonna (2014), TError: Towards a better quantification of the uncertainty propagated during the characterization of tephra deposits, *Stat. Volcanol.*, *1*, 1–27.
- Bonadonna, C., and A. Costa (2012), Estimating the volume of tephra deposits: A new simple strategy, *Geology*, *40*(5), 415–418.
- Bonadonna, C., and B. Houghton (2005), Total grain-size distribution and volume of tephra-fall deposits, *Bull. Volcanol.*, *67*, 441–456.
- Bonadonna, C., G. Ernst, and R. Sparks (1998), Thickness variations and volume estimates of tephra fall deposits: The importance of particle Reynolds number, *J. Volcanol. Geotherm. Res.*, *81*, 173–187.
- Bonadonna, C., et al. (2002), Tephra fallout in the eruption of Soufrière Hills Volcano, Montserrat, *Geol. Soc. Spec. Publ.*, London, U. K. *21*, 483–516.
- Brand, B. D., C. Mackaman-Lofland, N. M. Pollock, S. Bendaña, B. Dawson, and P. Wichgers (2014), Dynamics of pyroclastic density currents: Conditions that promote substrate erosion and self-channelization - Mount St Helens, Washington (USA), *J. Volcanol. Geotherm. Res.*, *276*, 189–214.
- Branney, M. J., and B. P. Kokelaar (2002), Pyroclastic density currents and the sedimentation of ignimbrites, *Geol. Soc. Mem.*, *27*, 152 pp.
- Brown, S. K., H. S. Crossweller, R. S. J. Sparks, E. Cottrell, N. I. Deligne, N. O. Guerrero, L. Hobbs, K. Kiyosugi, S. C. Loughlin, and L. Siebert (2014), Characterisation of the Quaternary eruption record: Analysis of the Large Magnitude Explosive Volcanic Eruptions (LaMEVE) database, *J. Appl. Volcanol.*, *3*, 1–22.
- Burgisser, A., S. Poussineau, L. Arbaret, T. H. Druitt, T. Giachetti, and J.-L. Bourdier (2010), Pre-explosive conduit conditions of the 1997 Vulcanian explosions at Soufrière Hills Volcano, Montserrat: I. Pressure and vesicularity distributions, *J. Volcanol. Geotherm. Res.*, *194*, 27–41.
- Carazzo, G., E. Kaminski, and S. Tait (2008), On the rise of turbulent plumes: Quantitative effects of variable entrainment for submarine hydrothermal vents, terrestrial and extra-terrestrial explosive volcanism, *J. Geophys. Res.*, *113*, B09201, doi:10.1029/2007JB005458.
- Carazzo, G., E. Kaminski, and S. Tait (2015), The timing and intensity of column collapse during explosive volcanic eruptions, *Earth Planet. Sci. Lett.*, *411*, 208–217.
- Carey, S., and H. Sigurdsson (1986), The 1982 eruptions of El Chichon volcano, Mexico (2): Observations and numerical modelling of tephra-fall distribution, *Bull. Volcanol.*, *48*, 127–141.
- Cas, R. A., and J. V. Wright (1987), *Volcanic Successions, Modern and Ancient: A Geological Approach to Processes, Products, and Successions*, Allen and Unwin., St Leonards, NSW.
- Cashman, K. V. (1992), Groundmass crystallization of Mount St. Helens dacite, 1980–1986: A tool for interpreting shallow magmatic processes, *Contrib. Mineral. Petrol.*, *109*, 431–449.
- Cashman, K. V., and B. Scheu (2015), Magmatic fragmentation, in *The Encyclopedia of Volcanoes*, edited by H. Sigurdsson et al., pp. 459–471, Elsevier, U. K.

- Charbonnier, S. J., and R. Gertisser (2008), Field observations and surface characteristics of pristine block-and-ash flow deposits from the 2006 eruption of Merapi Volcano, Java, Indonesia, *J. Volcanol. Geotherm. Res.*, *177*, 971–982.
- Charbonnier, S. J., and R. Gertisser (2011), Deposit architecture and dynamics of the 2006 block-and-ash flows of Merapi Volcano, Java, Indonesia, *Sedimentology*, *58*, 1573–1612.
- Charbonnier, S. J., A. Germa, C. B. Connor, R. Gertisser, K. Preece, J. C. Komorowski, F. Lavigne, T. Dixon, and L. Connor (2013), Evaluation of the impact of the 2010 pyroclastic density currents at Merapi volcano from high-resolution satellite imagery, field investigations and numerical simulations, *J. Volcanol. Geotherm. Res.*, *261*, 295–315.
- Cobenas, G., Thouret, J.-C., C. Bonadonna, and P. Boivin (2014), Reply to comment on: "The c. 2030 yr BP Plinian eruption of El Misti volcano, Peru: Eruption dynamics and hazard implications. Journal of Volcanology and Geothermal Research 241–242, 105–120." by Harpel et al., *JVGR 2013, J. Volcanol. Geotherm. Res.*, *275*, 103–113.
- Cole, P. D., E. Fernandez, E. Duarte, and A. M. Duncan (2005), Explosive activity and generation mechanisms of pyroclastic flows at Arenal volcano, Costa Rica between 1987 and 2001, *Bull. Volcanol.*, *67*, 695–716.
- Coltelli, M., P. Del Carlo, and L. Vezzoli (1998), Discovery of a Plinian basaltic eruption of Roman age at Etna volcano, Italy, *Geology*, *26*, 1095–1098.
- Cook, G. W., J. A. Wolff, and S. Self (2016), Estimating the eruptive volume of a large pyroclastic body: The Otowi Member of the Bandelier Tuff, Valles caldera, New Mexico, *Bull. Volcanol.*, *78*, 1–11.
- Costantini, L., L. Pioli, C. Bonadonna, J. Clavero, and C. Longchamp (2011), A late Holocene explosive mafic eruption of Villarrica volcano, Southern Andes: The Chaimilla deposit, *J. Volcanol. Geotherm. Res.*, *200*, 143–158.
- Davies, D. K., M. W. Quearry, and S. B. Bonis (1978), Glowing avalanches from the 1974 eruption of the volcano Fuego, Guatemala, *Geol. Soc. Am. Bull.*, *89*, 369–384.
- Di Muro, A., A. Neri, and M. Rosi (2004), Contemporaneous convective and collapsing eruptive dynamics: The transitional regime of explosive eruptions, *Geophys. Res. Lett.*, *31*, L10607, doi:10.1029/2004GL019709.
- Di Roberto, A., A. Bertagnini, M. Pompilio, and M. Bisson (2014), Pyroclastic density currents at Stromboli volcano (Aeolian Islands, Italy): A case study of the 1930 eruption, *Bull. Volcanol.*, *76*, 1–14.
- Douillet, G., et al. (2013), Sedimentology and geomorphology of the deposits from the August 2006 pyroclastic density currents at Tungurahua volcano, Ecuador, *Bull. Volcanol.*, *75*, 1–21.
- Druitt, T., S. Young, B. Baptie, C. Bonadonna, E. Calder, A. Clarke, P. Cole, C. Harford, R. Herd, and R. Luckett (2002), Episodes of cyclic Vulcanian explosive activity with fountain collapse at Soufrière Hills Volcano, Montserrat, *Geol. Soc. Spec. Publ.*, *21*, 281–306.
- Engwell, S., and J. Eychenne (2016), Contribution of fine ash to the atmosphere from plumes associated with pyroclastic density currents, in *Volcanic Ash: Hazard Observation*, edited by S. Mackie et al., pp. 67–88, Elsevier, U. K.
- Eychenne, J., and J.-L. Le Pennec (2012), Sigmoidal particle density distribution in a subplinian scoria fall deposit, *Bull. Volcanol.*, *74*, 2243–2249.
- Eychenne, J., Le Pennec, J.-L., L. Troncoso, M. Gouhier, and J.-M. Nedelec (2012), Causes and consequences of bimodal grain-size distribution of tephra fall deposited during the August 2006 Tungurahua eruption (Ecuador), *Bull. Volcanol.*, *74*, 187–205.
- Eychenne, J., J.-L. Le Pennec, P. Ramón, and H. Yepes (2013), Dynamics of explosive paroxysms at open-vent andesitic systems: High-resolution mass distribution analyses of the 2006 Tungurahua fall deposit (Ecuador), *Earth Planet. Sci. Lett.*, *361*, 343–355.
- Fee, D., M. Garces, and A. Steffke (2010), Infrasound from Tungurahua Volcano 2006–2008: Strombolian to Plinian eruptive activity, *J. Volcanol. Geotherm. Res.*, *193*, 67–81.
- Fierstein, J., and M. Nathenson (1992), Another look at the calculation of fallout tephra volumes, *Bull. Volcanol.*, *54*, 156–167.
- Fitzgerald, R., K. Tsunematsu, B. Kennedy, E. Breard, G. Lube, T. Wilson, A. Jolly, J. Pawson, M. Rosenberg, and S. Cronin (2014), The application of a calibrated 3D ballistic trajectory model to ballistic hazard assessments at Upper Te Maari, Tongariro, *J. Volcanol. Geotherm. Res.*, *286*, 248–262.
- Gardner, C. A., C. A. Neal, R. B. Waitt, and R. J. Janda (1994), Proximal pyroclastic deposits from the 1989–1990 eruption of Redoubt Volcano, Alaska—Stratigraphy, distribution, and physical characteristics, *J. Volcanol. Geotherm. Res.*, *62*, 213–250.
- Guffanti, M., G. C. Mayberry, T. J. Casadevall, and R. Wunderman (2009), Volcanic hazards to airports, *Nat. Hazards*, *51*, 287–302.
- Gurioli, L., B. F. Houghton, K. V. Cashman, and R. Cioni (2005), Complex changes in eruption dynamics during the 79 AD eruption of Vesuvius, *Bull. Volcanol.*, *67*, 144–159.
- Gurioli, L., R. Sulpizio, R. Cioni, A. Sbrana, R. Santacroce, W. Luperini, and D. Andronico (2010), Pyroclastic flow hazard assessment at Somma-Vesuvius based on the geological record, *Bull. Volcanol.*, *72*, 1021–1038.
- Gurioli, L., A. J. L. Harris, L. Colò, J. Bernard, M. Favalli, M. Ripepe, and D. Andronico (2013), Classification, landing distribution, and associated flight parameters for a bomb field emplaced during a single major explosion at Stromboli, Italy, *Geology*, *41*, 559–562.
- Hall, M., and P. Mothes (2008), The rhyolitic-andesitic eruptive history of Cotopaxi volcano, Ecuador, *Bull. Volcanol.*, *70*, 675–702.
- Hall, M., P. Ramon, P. Mothes, J. L. LePennec, A. Garcia, P. Samaniego, and H. Yepes (2004), Volcanic eruptions with little warning: The case of Volcán Reventador's Surprise November 3, 2002 Eruption, Ecuador, *Rev. Geol. Chile*, *31*, 349–358.
- Hall, M. L., A. L. Steele, P. A. Mothes, and M. C. Ruiz (2013), Pyroclastic density currents (PDC) of the 16–17 August 2006 eruptions of Tungurahua volcano, Ecuador: Geophysical registry and characteristics, *J. Volcanol. Geotherm. Res.*, *265*, 78–93.
- Hildreth, W., and R. E. Drake (1992), Volcán Quizapu, Chilean Andes, *Bull. Volcanol.*, *54*, 93–125.
- Horwell, C. J., and P. J. Baxter (2006), The respiratory health hazards of volcanic ash: A review for volcanic risk mitigation, *Bull. Volcanol.*, *69*, 1–24.
- Houghton, B., and C. Wilson (1989), A vesicularity index for pyroclastic deposits, *Bull. Volcanol.*, *51*, 451–462.
- Jaupart, C. (1998), Gas loss from magmas through conduit walls during eruption, *Geol. Soc. Spec. Publ.*, *145*, 73–90.
- Jaupart, C., and C. J. Allègre (1991), Gas content, eruption rate and instabilities of eruption regime in silicic volcanoes, *Earth Planet. Sci. Lett.*, *102*, 413–429.
- Jenkins, S., J.-C. Komorowski, P. Baxter, R. Spence, A. Picquout, and F. Lavigne (2013), The Merapi 2010 eruption: An interdisciplinary impact assessment methodology for studying pyroclastic density current dynamics, *J. Volcanol. Geotherm. Res.*, *261*, 316–329.
- Jordan, S., J.-L. Le Pennec, L. Gurioli, O. Roche, and P. Boivin (2016), Highly explosive eruption of the monogenetic 8.6 ka BP La Vache et Lassolas scoria cone complex (Chaîne des Puys, France), *J. Volcanol. Geotherm. Res.*, *313*, 15–28.
- Kaminski, E., and C. Jaupart (1998), The size distribution of pyroclasts and the fragmentation sequence in explosive volcanic eruptions, *J. Geophys. Res.*, *103*, 29,759–29,779.
- Kelfoun, K., P. Samaniego, P. Palacios, and D. Barba (2009), Testing the suitability of frictional behaviour for pyroclastic flow simulation by comparison with a well-constrained eruption at Tungurahua volcano (Ecuador), *Bull. Volcanol.*, *71*, 1057–1075.
- Klawonn, M., L. Frazer, C. Wolfe, B. Houghton, and M. Rosenberg (2014), Constraining particle size-dependent plume sedimentation from the 17 June 1996 eruption of Ruapehu Volcano, New Zealand, using geophysical inversions, *J. Geophys. Res. Solid Earth*, *119*, 1749–1763, doi:10.1002/2013JB010387.

- Komorowski, J.-C., Y. Legendre, B. Caron, and G. Boudon (2008), Reconstruction and analysis of sub-plinian tephra dispersal during the 1530 AD Soufriere (Guadeloupe) eruption: Implications for scenario definition and hazards assessment, *J. Volcanol. Geotherm. Res.*, *178*, 491–515.
- Kueppers, U., C. Cimarelli, K.-U. Hess, J. Taddeucci, F. B. Wadsworth, and D. B. Dingwell (2014), The thermal stability of Eyjafjallajökull ash versus turbine ingestion test sands, *J. Appl. Volcanol.*, *3*, 1–11.
- Le Pennec, J.-L., D. Hermitte, I. Dana, P. Pezard, C. Coulon, J. J. Cochemé, E. Mulyadi, F. Ollagnier, and C. Revest (2001), Electrical conductivity and pore-space topology of Merapi lavas: Implications for the degassing of porphyritic andesite magmas, *Geophys. Res. Lett.*, *28*, 4283–4286.
- Le Pennec, J.-L., G. A. Ruiz, P. Ramón, E. Palacios, P. Mothes, and H. Yepes (2012), Impact of tephra falls on Andean communities: The influences of eruption size and weather conditions during the 1999–2001 activity of Tungurahua volcano, Ecuador, *J. Volcanol. Geotherm. Res.*, *217–218*, 91–103.
- Lube, G., S. J. Cronin, T. Platz, A. Freundt, J. N. Procter, C. Henderson, and M. F. Sheridan (2007), Flow and deposition of pyroclastic granular flows: A type example from the 1975 Ngauruhoe eruption, New Zealand, *J. Volcanol. Geotherm. Res.*, *161*, 165–186.
- Major, J. J., and L. E. Lara (2013), Overview of Chaitén Volcano, Chile, and its 2008–2009 eruption, *Andean Geol.*, *40*, 196–215.
- Marzocchi, W., L. Sandri, P. Gasparini, C. Newhall, and E. Boschi (2004), Quantifying probabilities of volcanic events: The example of volcanic hazard at Mount Vesuvius, *J. Geophys. Res.*, *109*, B11201, doi:10.1029/2004JB003155.
- McGimsey, R. G., C. Neal, and C. M. Riley (2001), *Areal Distribution, Thickness, Mass, Volume, and Grain Size of Tephra-Fall Deposits From the 1992 Eruptions of Crater Peak Vent, Mt. Spurr Volcano, Alaska*, U.S. Geol. Surv., Alaska Volcano Obs, Anchorage, Alaska.
- Miller, T. P., C. Neal, and R. Waitt (1995), Pyroclastic flows of the 1992 Crater Peak eruptions: Distribution and origin, in *The 1992 Eruptions of Crater Peak vent, Mount Spurr Volcano, Alaska*, U.S. Geol. Surv. Bull., *2139*, edited by T. E. C. Keith, pp. 81–87, US Geol. Surv., Anchorage, Alaska.
- Moore, J. G., and W. G. Melson (1969), Nuées Ardentes of the 1968 Eruption of Mayon Volcano, Philippines, *Bull. Volcanol.*, *33*, 600–620.
- Nairn, I. A., and S. Self (1978), Explosive eruptions and pyroclastic avalanches from Ngauruhoe in February 1975, *J. Volcanol. Geotherm. Res.*, *3*, 39–60.
- Neri, A., A. Di Muro, and M. Rosi (2002), Mass partition during collapsing and transitional columns by using numerical simulations, *J. Volcanol. Geotherm. Res.*, *115*, 1–18.
- Newhall, C. G., and S. Self (1982), The Volcanic Explosivity Index (VEI) an estimate of explosive magnitude for historical volcanism, *J. Geophys. Res.*, *87*, 1231–1238.
- Pioli, L., E. Erlund, E. Johnson, K. Cashman, P. Wallace, M. Rosi, and H. D. Granados (2008), Explosive dynamics of violent Strombolian eruptions: The eruption of Parícutin Volcano 1943–1952 (Mexico), *Earth Planet. Sci. Lett.*, *271*, 359–368.
- Pistolesi, M., D. Delle Donne, L. Pioli, M. Rosi, and M. Ripepe (2011), The 15 March 2007 explosive crisis at Stromboli volcano, Italy: Assessing physical parameters through a multidisciplinary approach, *J. Geophys. Res.*, *116*, B12206, doi:10.1029/2011JB008527.
- Pyle, D. (1989), The thickness, volume and grainsize of tephra fall deposits, *Bull. Volcanol.*, *51*, 1–15.
- Pyle, D. (2000), Sizes of volcanic eruptions, *Encycl. Volcanoes*, *1*, 263–269.
- Rittmann, A. (1962), *Volcanoes and Their Activity*, Interscience Publishers, N. Y.
- Roche, O., J. C. Phillips, and K. Kelfoun (2013), Pyroclastic density currents, in *Modeling Volcanic Processes: The Physics and Mathematics of Volcanism*, edited by S. A. Fagents, T. K. P. Gregg, and R. M. C. Lopes, pp. 203–229, Cambridge Univ. Press, U. K.
- Rose, W. I., S. Self, P. J. Murrow, C. Bonadonna, A. J. Durant, and G. G. J. Ernst (2008), Nature and significance of small volume fall deposits at composite volcanoes: Insights from the October 14, 1974 Fuego eruption, Guatemala, *Bull. Volcanol.*, *70*, 1043–1067.
- Rosi, M., A. Bertagnini, A. Harris, L. Pioli, M. Pistolesi, and M. Ripepe (2006), A case history of paroxysmal explosion at Stromboli: Timing and dynamics of the April 5, 2003 event, *Earth Planet. Sci. Lett.*, *243*, 594–606.
- Rust, A. C., and K. V. Cashman (2011), Permeability controls on expansion and size distributions of pyroclasts, *J. Geophys. Res.*, *116*, B11202, doi:10.1029/2011JB008494.
- Sahagian, D. L., and A. A. Proussevitch (1998), 3D particle size distributions from 2D observations: Stereology for natural applications, *J. Volcanol. Geotherm. Res.*, *84*, 173–196.
- Samaniego, P., J.-L. Le Pennec, C. Robin, and S. Hidalgo (2011), Petrological analysis of the pre-eruptive magmatic process prior to the 2006 explosive eruptions at Tungurahua volcano (Ecuador), *J. Volcanol. Geotherm. Res.*, *199*, 69–84.
- Sarna-Wojcicki, A. M., S. Shipley, R. B. Waitt Jr., D. Dzurisin, and S. H. Wood (1981), Areal distribution, thickness, mass, volume, and grain size of air-fall ash from the six major eruptions of 1980, The 1980 Eruptions of Mount St. Helens, pp. 577–600, Wash.
- Saucedo, R., J. L. Macías, M. I. Bursik, J. C. Mora, J. C. Gavilanes, and A. Cortes (2002), Emplacement of pyroclastic flows during the 1998–1999 eruption of Volcán de Colima, México, *J. Volcanol. Geotherm. Res.*, *117*, 129–153.
- Saucedo, R., J. Macías, and M. Bursik (2004), Pyroclastic flow deposits of the 1991 eruption of Volcán de Colima, Mexico, *Bull. Volcanol.*, *66*, 291–306.
- Scasso, R. A., H. Corbella, and P. Tiberi (1994), Sedimentological analysis of the tephra from the 12–15 August 1991 eruption of Hudson volcano, *Bull. Volcanol.*, *56*, 121–132.
- Schwarzkopf, L. M., H.-U. Schmincke, and S. J. Cronin (2005), A conceptual model for block-and-ash flow basal avalanche transport and deposition, based on deposit architecture of 1998 and 1994 Merapi flows, *J. Volcanol. Geotherm. Res.*, *139*, 117–134.
- Scott, W. E., and R. G. McGimsey (1994), Character, mass, distribution, and origin of tephra-fall deposits of the 1989–1990 eruption of Redoubt Volcano, south-central Alaska, *J. Volcanol. Geotherm. Res.*, *62*, 251–272.
- Scott, W. E., R. P. Hoblitt, R. C. Torres, S. Self, M. M. L. Martinez, and T. Nillos (1996), Pyroclastic flows of the June 15, 1991, climactic eruption of Mount Pinatubo, in *Fire and Mud: Eruptions and Lahars of Mount Pinatubo, Philippines*, edited by C. G. Newhall, and R. Punongbayan, pp. 545–570, Philippine Institute of Volcanology and Seismology, Quezon City.
- Self, S., and M. R. Rampino (2012), The 1963–1964 eruption of Agung volcano (Bali, Indonesia), *Bull. Volcanol.*, *74*, 1521–1536.
- Shea, T., B. F. Houghton, L. Gurioli, K. V. Cashman, J. E. Hammer, and B. J. Hobden (2010), Textural studies of vesicles in volcanic rocks: An integrated methodology, *J. Volcanol. Geotherm. Res.*, *190*, 271–289.
- Siebert, L., T. Simkin, and P. Kimberly (2011), *Volcanoes of the World*, Univ. of Calif. Press, USA.
- Sigurdsson, H., S. N. Carey, and J. M. Espindola (1984), The 1982 eruptions of El Chichón Volcano, Mexico: Stratigraphy of pyroclastic deposits, *J. Volcanol. Geotherm. Res.*, *23*, 11–37.
- Sigurdsson, H., S. Carey, and R. Fisher (1987), The 1982 eruptions of El Chichón volcano, Mexico (3): Physical properties of pyroclastic surges, *Bull. Volcanol.*, *49*, 467–488.
- Solikhin, A., V. Pinel, J. Vandemeulebrouck, J.-C. Thouret, and M. Hendrasto (2015), Mapping the 2010 Merapi pyroclastic deposits using dual-polarization Synthetic Aperture Radar (SAR) data, *Remote Sens. Environ.*, *158*, 180–192.
- Sparks, R., and L. Wilson (1976), A model for the formation of ignimbrite by gravitational column collapse, *J. Geol. Soc.*, *132*, 441–451.

- Sparks, R. S. J., M. C. Gardeweg, E. S. Calder, and S. J. Matthews (1997), Erosion by pyroclastic flows on Lascar Volcano, Chile, *Bull. Volcanol.*, *58*, 557–565.
- Steffke, A. M., D. Fee, M. Garces, and A. Harris (2010), Eruption chronologies, plume heights and eruption styles at Tungurahua Volcano: Integrating remote sensing techniques and infrasound, *J. Volcanol. Geotherm. Res.*, *193*, 143–160.
- Tanguy, J. C., C. Ribière, A. Scarth, and W. S. Tjetjep (1998), Victims from volcanic eruptions: A revised database, *Bull. Volcanol.*, *60*, 137–144.
- Wadge, G., D. Oramas Dorta, and P. D. Cole (2006), The magma budget of Volcán Arenal, Costa Rica from 1980 to 2004, *J. Volcanol. Geotherm. Res.*, *157*, 60–74.
- Walker, G. P. L. (1971), Grain-size characteristics of pyroclastic deposits, *J. Geol.*, *79*, 696–714.
- Watts, R., R. Herd, R. Sparks, and S. Young (2002), Growth patterns and emplacement of the andesitic lava dome at Soufriere Hills Volcano, Montserrat, *Geol. Soc. Spec. Publ.*, *21*, 115–152.
- Waythomas, C. F., M. M. Haney, D. Fee, D. J. Schneider, and A. Wech (2014), The 2013 eruption of Pavlof Volcano, Alaska: A spatter eruption at an ice-and snow-clad volcano, *Bull. Volcanol.*, *76*, 1–12.
- Wiesner, M., A. Wetzel, S. Catane, E. Listanco, and H. Mirabueno (2004), Grain size, areal thickness distribution and controls on sedimentation of the 1991 Mount Pinatubo tephra layer in the South China Sea, *Bull. Volcanol.*, *66*, 226–242.
- Wilson, L., and G. Walker (1987), Explosive volcanic eruptions-VI. Ejecta dispersal in plinian eruptions: The control of eruption conditions and atmospheric properties, *Geophys. J. Int.*, *89*, 657–679.
- Wright, H. M., K. V. Cashman, P. A. Mothes, M. L. Hall, A. G. Ruiz, and J. L. Le Pennec (2012), Estimating rates of decompression from textures of erupted ash particles produced by 1999–2006 eruptions of Tungurahua volcano, Ecuador, *Geology*, *40*, 619–622.
- Yamamoto, T., S. Takarada, and S. Suto (1993), Pyroclastic flows from the 1991 eruption of Unzen volcano, Japan, *Bull. Volcanol.*, *55*, 166–175.